ELSEVIER

Volume 180, Number 5, May 2007

JOURNAL OF SOLID STATE CHEMISTRY

www.elsevier.com/locate/jssc

CONTENTS

Abstracted/indexed in BioEngineering Abstracts, Chemical Abstracts, Coal Abstracts, Current Contents/Physics, Chemical, & Earth Sciences, Engineering Index, Research Alert, SCISEARCH, Science Abstracts, and Science Citation Index. Also covered in the abstract and citation database SCOPUS®. Full text available on ScienceDirect®.

Regular Articles

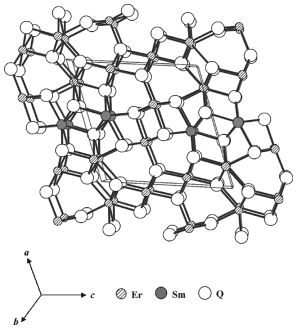

The structure of Er_3SmSe_6 viewed approximately down [010].

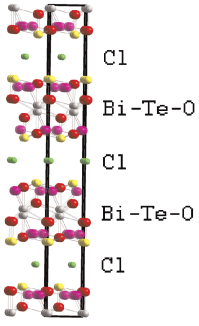

A new bismuth tellurium oxychloride $Bi_{0.87}Te_2O_{4.9}Cl_{0.87}$ has been synthesized. The compound has a new type of layered structure.

Regular Articles—Continued

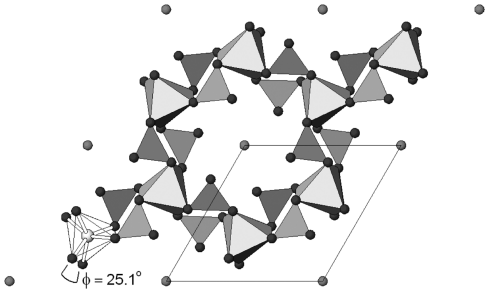

A solid–state reaction between $SrCO_3$, Cr_2O_3 and SrF_2 produced $Sr_{10}(CrO_4)_6F_2$ apatite and Sr_2CrO_4 which adopts the K_2NiF_4-type structure. Powder X-ray and electron diffraction confirmed that Sr_2CrO_4 is body-centred tetragonal, while a combination of neutron and X-ray diffraction verified $Sr_{10}(CrO_4)_6F_2$ is hexagonal. X-ray photoelectron spectroscopy and magnetic measurements identified the oxidation states of chromium in these phases.

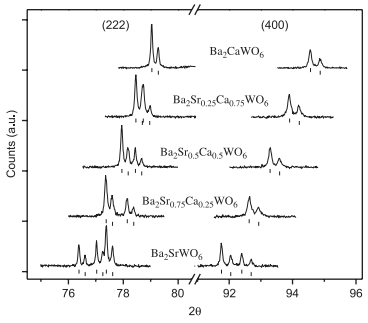

Enlarged sections showing the evolution of the basic (222) and (400) reflections in $Ba_2Sr_{1-x}Ca_xWO_6$. Tick marks below are the positions of Bragg's reflections calculated using the space groups $I2/m$ ($x=0$), $R\bar{3}$ ($x=0.25$, 0.5 and 0.75) and $Fm\bar{3}m$ ($x=1$), respectively.

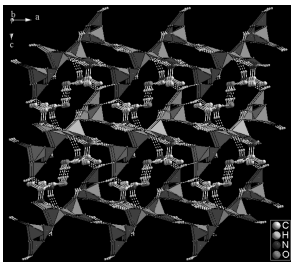

One new organically templated borate $[NH_3CH_2CHCH_3NH_3]][B_8O_{11}(OH)_4]\cdot H_2O$ **1**, has been synthesized under mild hydrothermal conditions. Its structure features an unusual open-branched borate chain constructed from $[B_3O_6(OH)]$ groups, onto which the $[B_5O_7(OH)_3]$ groups are grafted. It is the first instance of 1D borate templated by the organic amine. Adjacent borate chains are linked together by multipoint bonds to form interesting three-dimensional network with rhombus-like channels, in which the guest water and diprotonated organic amine molecules reside.

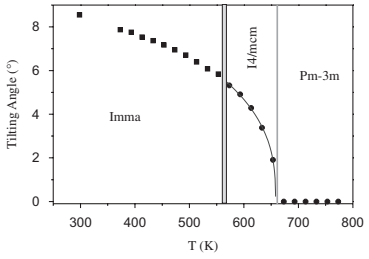

Temperature dependence of the octahedral tilting angles in $BaPbO_3$. The continuous line in tetragonal phase region is the fit to the expression: $\varphi = A(T_c - T)^{\beta}$ with the fitted values of $T_c = 658(1)$ K, $\beta = 0.36(2)$ and $A = 1.1(1)$. The shaded area indicates the possible two-phase region.

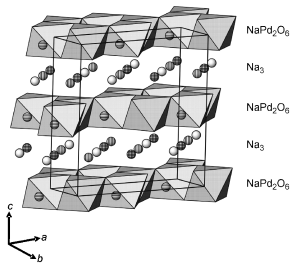

Na_2PdO_3 (space group $C2/c$, $a = 5.3857(1)$ Å, $b = 9.3297(1)$ Å, $c = 10.8136(2)$ Å, $\beta = 99.437(2)$, $Z = 8$) belongs to the Li_2RuO_3-structure type, being the layered variant of the NaCl structure, where the layers of octahedral interstices filled with Na^+ and Pd^{4+} cations ($NaPd_2O_6$ slabs) alternate with Na_3 layers along the c-axis.

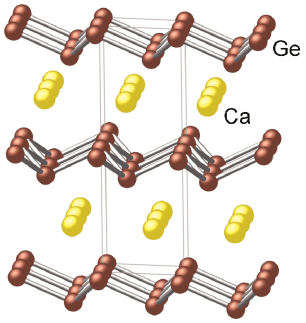

Reported are the synthesis, the structure and the band structure analysis of a new polymorph of $CaGe_2$ (α-$CaGe_2$). The similarities and the differences between this compound and the known rhombohedral β-$CaGe_2$ are discussed in detail. LMTO calculations suggest that in spite of the apparent adherence to the Zintl rules for electron counting, α-$CaGe_2$ is metallic due to a small cation–anion orbital mixing.

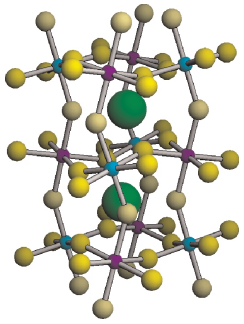

The title double perovskites are monoclinic, space group $P2_1/n$, and the magnetic properties suggest the possibility of a partial charge disproportionation $B'^{2+} + U^{6+} \Leftrightarrow B'^{3+} + U^{5+}$, accounting for plausible ferrimagnetic interactions between B' and U sublattices.

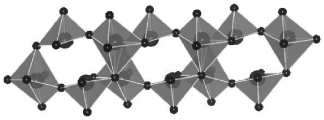

Zinc dimolybdate $ZnMo_2O_7\cdot 5H_2O$ was synthesized and its crystal structure has been solved by X-ray powder diffraction methods. The IR and TGA/DTA studies were performed. A study of thermal decomposition in situ of $ZnMo_2O_7\cdot 5H_2O$ in air and nitrogen by X-ray diffraction was also performed.

Continued

$Pr_4B_{10}O_{21}$: A new composition of rare-earth borates by high-pressure/high-temperature synthesis
Almut Haberer, Gunter Heymann and Hubert Huppertz
Page 1595

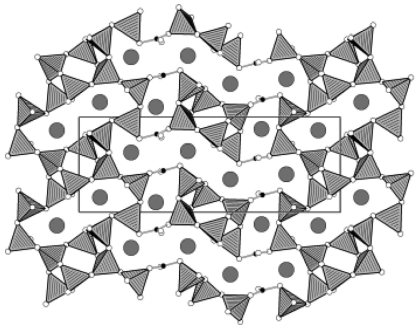

Synthesis of $Pr_4B_{10}O_{21}$ via the multianvil high-pressure/high-temperature technique representing a new composition of rare-earth borates.

Syntheses, structures, and properties of $Ag_4(Mo_2O_5)(SeO_4)_2(SeO_3)$ and $Ag_2(MoO_3)_3SeO_3$
Jie Ling and Thomas E. Albrecht-Schmitt
Page 1601

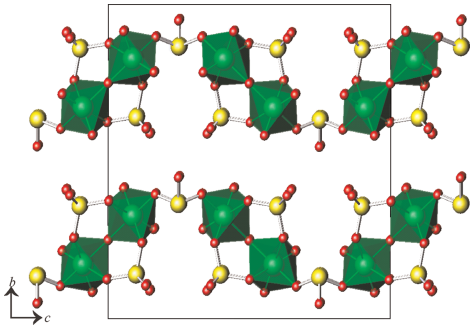

A view of the one-dimensional $[(Mo_2O_5)(SeO_4)_2(SeO_3)]^{4-}$ chains that extend down the *c*-axis in the structure of $Ag_4(Mo_2O_5)(SeO_4)_2(SeO_3)$.

Charge compensation and oxidation in $Na_xCoO_{2-\delta}$ and $Li_xCoO_{2-\delta}$ studied by XANES
M. Valkeapää, Y. Katsumata, I. Asako, T. Motohashi, T.S. Chan, R.S. Liu, J.M. Chen, H. Yamauchi and M. Karppinen
Page 1608

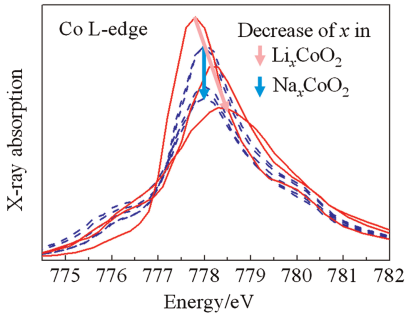

The valence of cobalt increases more upon removal of alkali metal from Li_xCoO_2 than from Na_xCoO_2.

Two $Ce(SO_4)_2 \cdot 4H_2O$ polymorphs: Crystal structure and thermal behavior
Barbara M. Casari and Vratislav Langer
Page 1616

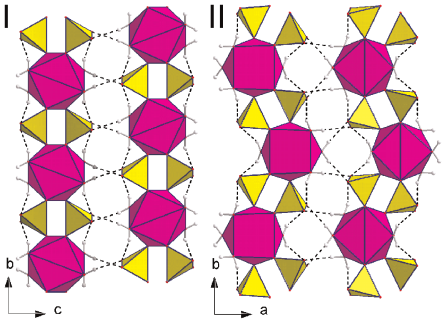

The cerium atoms are eight-coordinated in both α-$Ce(SO_4)_2 \cdot 4H_2O$ (I) and β-$Ce(SO_4)_2 \cdot 4H_2O$ (II) forming slightly distorted square antiprisms, but the mutual position of the ligands differs, resulting in stereoisomerism. Both structures are built up by layers of $Ce(H_2O)_4(SO_4)_2$ held together by a hydrogen bonding network.

Magnetic structures of the M_2TbF_6 (M = Li, K, Rb) fluorides: A complex behavior resulting from frustration
M. Josse, M. El-Ghozzi, D. Avignant, G. André and F. Bourée
Page 1623

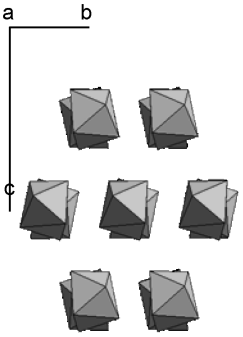

Pseudo-hexagonal packing of the $[TbF_6]^{2-}$ chains in Li_2TbF_6.

Synthesis and characterization of sulfate and dodecylbenzenesulfonate intercalated zinc–iron layered double hydroxides by one-step coprecipitation route
Hui Zhang, Xing Wen and Yingxia Wang
Page 1636

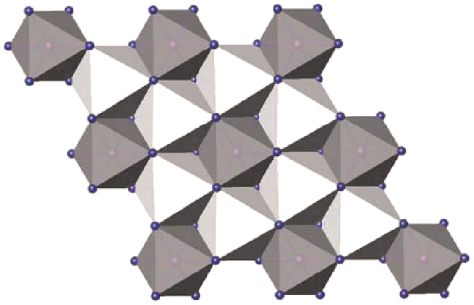

For Zn^{2+}–Fe^{2+}–Fe^{3+} GR2(SO_4^{2-}), according to the derived chemical formula, Fe^{3+} was arranged at 1*a* (0, 0, 0) position, while all Zn^{2+} were in 2*d* position with the occupancy 0.645, and the left part of 2*d* positions were taken by Fe^{2+}/Fe^{3+}.

Three new 2-D metal-organic frameworks containing 1-D metal chains bridged by *N*-benzesulfonyl-glutamic acid: Syntheses, crystal structures and properties

Lu-Fang Ma, Xian-Kuan Huo, Li-Ya Wang, Jian-Ge Wang and Yao-Ting Fan

Page 1648

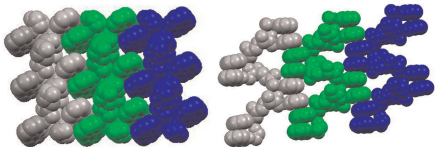

Three new complexes, $[Cd(bsglu)(bipy)]_n$ (**1**), $[Cd(bsglu)\cdot(H_2O)]_n$ (**2**) and $\{[Cu_2(bsglu)_2(bipy)_2]\cdot 4H_2O\}_n$ (**3**), constructed from Cd(II) or Cu(II) salt with *N*-benzesulfonyl-glutamic acid were synthesized and characterized. Compounds **1** and **3** exhibit one-dimensional chains which are further connected to form two-dimensional supramolecular networks through π–π aromatic stacking interactions in a novel zipper-like way. Compound **2** presents a two-dimensional layer structure. Luminescence of **1** and magnetic properties of **3** are also investigated.

Synthesis and crystal structure of a novel pentaborate, $Na_3ZnB_5O_{10}$

Xuean Chen, Ming Li, Xinan Chang, Hegui Zang and Weiqiang Xiao

Page 1658

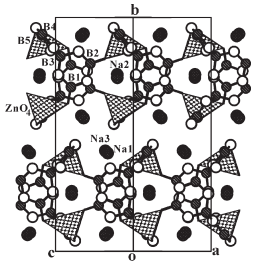

$Na_3ZnB_5O_{10}$ represents a new structure type in which double ring $[B_5O_{10}]^{5-}$ building units are bridged by ZnO_4 tetrahedra through common O atoms to form a two-dimensional $^2_\infty[ZnB_5O_{10}]^{3-}$ layer. *Symmetry-center* related $^2_\infty[ZnB_5O_{10}]^{3-}$ layers are stacked along the *b*-axis, with the interlayer void spaces and intralayer open channels filled by Na^+ cations.

Two-dimensional layer architecture assembled by Keggin polyoxotungstate, Cu(II)–EDTA complex and sodium linker: Synthesis, crystal structures, and magnetic properties

Hong Liu, Lin Xu, Guang-Gang Gao, Feng-Yan Li, Yan-Yan Yang, Zhi-Kui Li and Yu Sun

Page 1664

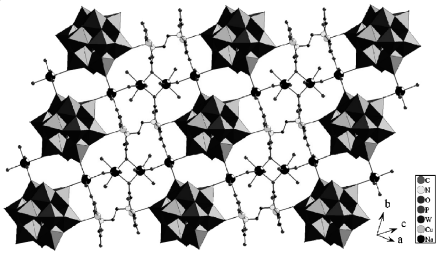

Two new polyoxometalate-based hybrids, $Na_4(OH)[Cu_2(EDTA)PW_{12}O_{40}]\cdot 17H_2O$ (**1**) and $Na_4[Cu_2(EDTA)SiW_{12}O_{40}]\cdot 19H_2O$ (**2**), have been synthesized and structurally characterized, which consist of one-dimensional chain structure assembled by Keggin polyoxotungstate and copper(II)–EDTA complex. The chains are further connected to form two-dimensional layer architecture assembled by the one-dimensional chain structure and sodium linker.

Structure and physical properties of BaCuTeF

Cheol-Hee Park, Robert Kykyneshi, Alexandre Yokochi, Janet Tate and Douglas A. Keszler

Page 1672

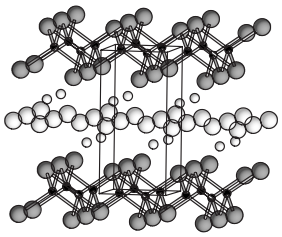

The telluride fluoride BaCuTeF has been synthesized and structurally characterized through Rietveld refinement of X-ray diffraction data. It crystallizes in the tetragonal structure of LaCuOS. Optical and transport measurements have been used to establish the material as a degenerate *p*-type semiconductor with a band gap near 2.3 eV.

Systematic study of photoluminescence upon band gap excitation in perovskite-type titanates $R_{1/2}Na_{1/2}TiO_3$:Pr (R = La, Gd, Lu, and Y)

Yoshiyuki Inaguma, Takeshi Tsuchiya and Tetsuhiro Katsumata

Page 1678

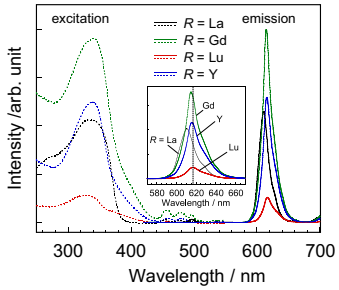

The red intense emission assigned to *f*–*f* transition of Pr^{3+} from the excited $^1D_2$ level to the ground $^3H_4$ state upon the band gap photo-excitation (UV) was observed upon the band gap photo-excitation in perovskites $R_{1/2}Na_{1/2}TiO_3$:Pr(R = La, Gd, Lu, and Y). It was found that the systematic changes in their luminescent properties are strongly dependent on the structure.

Hydrothermal synthesis, thermal, structural, spectroscopic and magnetic studies of the $Mn_{5-x}Co_x(HPO_4)_2(PO_4)_2(H_2O)_4$ (x = 1.25, 2, 2.5 and 3) finite solid solution

Edurne S. Larrea, José L. Mesa, José L. Pizarro, María I. Arriortua and Teófilo Rojo

Page 1686

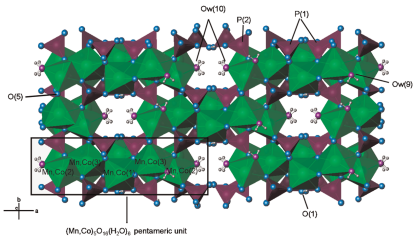

Crystal structutre of the finite solid solution $Mn_{5-x}Co_x$ $(HPO_4)_2$ $(PO_4)_2$ $(H_2O)_4$ (x = 1.25, 2, 2.5, 3).

Continued

Crystal structures, charge and oxygen-vacancy ordering in oxygen deficient perovskites $SrMnO_x$ ($x < 2.7$)

Leopoldo Suescun, Omar Chmaissem, James Mais, Bogdan Dabrowski and James D. Jorgensen

Page 1698

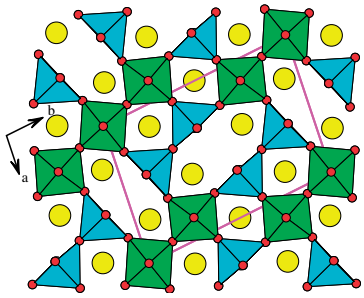

The structures of $Sr_5Mn_5O_{13}$ and $Sr_7Mn_7O_{19}$ (shown) were determined using synchrotron X-rays and neutron time-of-flight powder diffraction and the Rietveld method on multiphase bulk samples. Charge, orbital and oxygen vacancy-ordering has been observed in the novel compounds where Mn^{4+} octahedra and Mn^{3+} pyramids are linked through the corners leaving lines of vacant oxygen sites lying along the *c*-axis.

Syntheses and characterization of zero-dimensional molybdoantimonites, $A_2(Mo_4Sb_2O_{18})$ (A = Y, La, Nd, Sm, Gd and Dy)

G. Kalpana and K. Vidyasagar

Page 1708

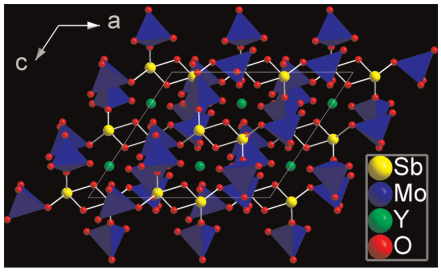

Six isostructural $A_2(Mo_4Sb_2O_{18})$ (A = Y, La, Nd, Sm, Gd and Dy) compounds, containing discrete, centrosymmetric anionic $(Mo_4Sb_2O_{18})^{6-}$ aggregates, exhibit characteristic Sb^{3+} photoluminescence.

Building up 3-D framework structure from interlinking layered cobalt phosphates and organic pillars

Wei-Kuo Chang, Ray-Kuang Chiang and Sue-Lein Wang

Page 1713

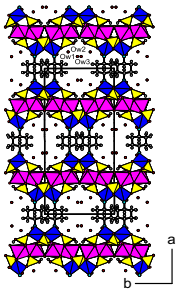

A new cobalt phosphate consists of cobalt phosphate layers and coordinated N-donor ligands, trans-1,4-diaminocyclohexane, which were interlinked to form a 3-D framework structure with 1-D tunnel occupied by water molecules.

Rare earth–transition metal–magnesium compounds—An overview

Ute Ch. Rodewald, Bernard Chevalier and Rainer Pöttgen

Page 1720

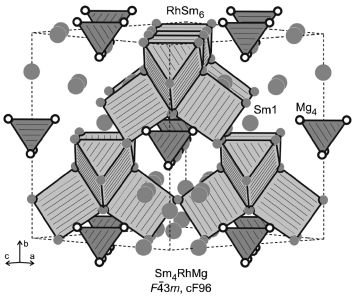

View of the Sm_4RhMg crystal structure approximately along the direction. Samarium, rhodium, and magnesium atoms are drawn as medium gray, filled (hidden in the trigonal prisms), and open circles, respectively. The three-dimensional network of corner-sharing $RhSm_6$ trigonal prisms and the Mg_4 tetrahedra are emphasized. The Sm1 atoms do not participate in the network of condensed trigonal prisms.

Cation distribution and ferromagnetic exchange in the $YMn_{0.5}Co_{0.5}O_3$ perovskite investigated by neutron powder diffraction

M. Mouallem-Bahout, T. Roisnel, G. André, C. Moure and O. Peña

Page 1737

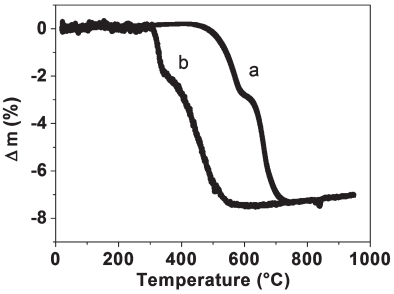

Thermogravimetric curves of hydrogen reduction of $YMn_{0.5}Co_{0.5}O_3$ (upper) and $YMn_{0.5}Ni_{0.5}O_3$ (lower) in $5\%H_2/N_2$ flow. Heating rate is 2°C/min.

Synthesis and photocatalytic activity for water-splitting reaction of nanocrystalline mesoporous titania prepared by hydrothermal method

Jaturong Jitputti, Sorapong Pavasupree, Yoshikazu Suzuki and Susumu Yoshikawa

Page 1743

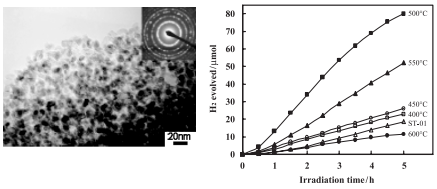

Nanocrystalline mesoporous TiO_2 was synthesized by hydrothermal method. The physical properties of the synthesized TiO_2 were thoroughly studied in relation to its photocatalytic activity for H_2 evolution from water-splitting reaction. It was found that the photocatalytic activity of synthesized TiO_2 treated with appropriate calcination temperature was considerably higher than that of commercial TiO_2 (Ishihara ST-01).

Three new tellurite halides with unusual Te^{4+} coordinations and iron honeycomb lattice variants
Richard Becker and Mats Johnsson
Page 1750

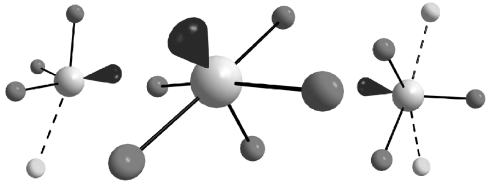

The crystal structure of three new iron and copper-iron tellurite halides are presented. All three compounds have layered crystal structures where the Fe atoms form variants of the honeycomb lattice as well as highly unusual Te^{4+} coordination polyhedra, e.g. $[TeO_3XE]$, $[TeO_{3+2}E]$, and $[TeO_3X_2E]$. The crystal structures contain large non-bonding volumes occupied by the stereochemically active lone–pair electrons on Te^{4+}.

Structural changes of Na_xCoO_2 ($x = 0.74$) at high pressures
F.X. Zhang, S.K. Saxena and C.S. Zha
Page 1759

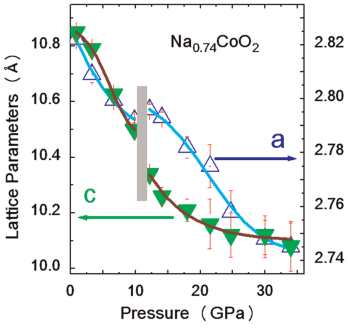

Pressure-induced structural change in γ-Na_xCoO_2 results in the discontinuity of lattice parameters.

Synthesis, crystal and band structures, and optical properties of a new lanthanide–alkaline earth tellurium(IV) oxide: $La_2Ba(Te_3O_8)(TeO_3)_2$
Hai-Long Jiang, Fang Kong and Jiang-Gao Mao
Page 1764

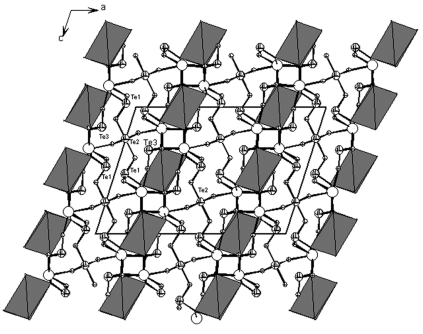

A new quaternary lanthanide alkaline–earth tellurium(IV) oxide, $La_2Ba(Te_3O_8)(TeO_3)_2$, has been prepared by the solid-state reaction and structurally characterized. The structure of $La_2Ba(Te_3O_8)(TeO_3)_2$ is 3D network in which the cationic $[La_2Ba(TeO_3)_2]^{4+}$ layers are cross-linked by $Te_3O_8^{4-}$ anions. Both band structure calculation by the DFT method and optical diffuse reflectance spectrum measurements indicate that $La_2Ba(Te_3O_8)(TeO_3)_2$ is a wide band-gap semiconductor.

Synthesis, structure and magnetic properties of new vanadate $PbCo_2V_2O_8$
Zhangzhen He, Yutaka Ueda and Mitsuru Itoh
Page 1770

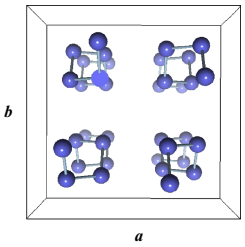

A structural arrangement of isolated Co^{2+} ions in $PbCo_2V_2O_8$ with spiral chain along the *c*-axis is clearly seen, where the nearest-neighbor chains screw adversely each other with right or left manner.

Synthesis of layered cathode material $Li[Co_xMn_{1-x}]O_2$ from layered double hydroxides precursors
Yanluo Lu, Min Wei, Lan Yang and Congju Li
Page 1775

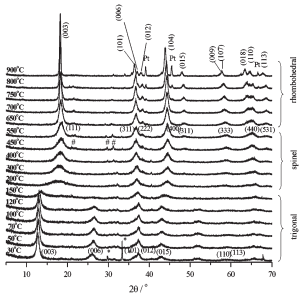

In situ HT-XRD and TG–MS were used to monitor the structural transformation during the reaction of CoMn LDHs and $LiOH \cdot H_2O$: firstly the layered structure of LDHs transformed to an intermediate phase with spinel structure; then intercalation of Li^+ occurred, which results in the formation of layered $Li[Co_xMn_{1-x}]O_2$ with α-$NaFeO_2$ structure. The structure and the electrochemical properties of $Li[Co_xMn_{1-x}]O_2$ were studied.

Rapid Communications

The mechanism of reequilibration of solids in the presence of a fluid phase
Andrew Putnis and Christine V. Putnis
Page 1783

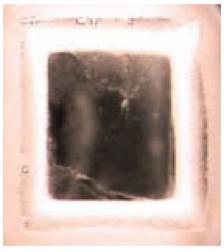

A single crystal of KBr is transformed to a porous single crystal of KCl by immersion in saturated KCl solution. The image shows partial transformation of a crystal of KBr (core) to KCl (porous, milky rim) by an interface coupled dissolution–reprecipitation mechanism. The external dimensions and crystallographic orientation of the original crystal are preserved, while a reaction interface moves through the crystal.

Continued

Synthesis of visible light-activated TiO_2 photocatalyst via surface organic modification

Dong Jiang, Yao Xu, Bo Hou, Dong Wu and Yuhan Sun

Page 1787

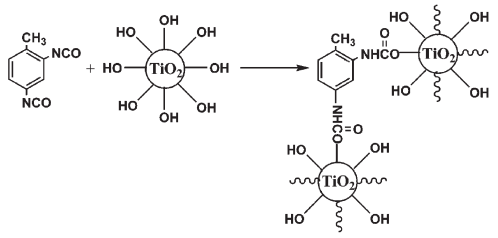

A visible light-activated TiO_2 photocatalyst was successfully synthesized by the surface organic modification to TiO_2. The surface hydroxyls of TiO_2 nanoparticles reacted with the active –NCO groups of tolylene diisocyanate (TDI) to form a surface complex. The TDI-modified TiO_2 photocatalysts showed higher activity for the photocatalytic degradation of methylene blue under visible light irradiation.

Photoluminescence properties of a novel phosphor, $Na_3La_9O_3(BO_3)_8$:RE^{3+} (RE = Eu,Tb)

Xiaoyan Bai, Guochun Zhang and Peizhen Fu

Page 1792

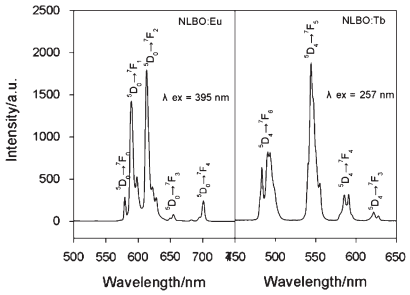

The dominated emission of NLBO:Eu located at 613 nm is from the electric dipole transition $^5D_0 \rightarrow {}^7F_2$. NLBO:Tb emit bright green luminescence centered at 544 nm attributed to the transition $^5D_4 \rightarrow {}^7F_5$. The concentration dependence of the emission intensity showed that the optimum doping concentration of Eu and Tb is 30% and 10%, respectively.

Author inquiries

Submissions

For detailed instructions on the preparation of electronic artwork, consult the journal home page at http://authors.elsevier.com.

Other inquiries

Visit the journal home page (http://authors.elsevier.com) for the facility to track accepted articles and set up e-mail alerts to inform you of when an article's status has changed. The journal home page also provides detailed artwork guidelines, copyright information, frequently asked questions and more.

Contact details for questions arising after acceptance of an article, especially those relating to proofs, are provided after registration of an article for publication.

Language Polishing

Authors who require information about language editing and copyediting services pre- and post-submission should visit http://www.elsevier.com/wps/find/authorshome.authors/languagepolishing or contact authorsupport@elsevier.com for more information. Please note Elsevier neither endorses nor takes responsibility for any products, goods, or services offered by outside vendors through our services or in any advertising. For more information please refer to our Terms & Conditions at http://www.elsevier.com/wps/find/termsconditions.cws_home/termsconditions.

For a full and complete Guide for Authors, please refer to *J. Solid State Chem.,* Vol. 180, Issue 1, pp. *bmi–bmv*. The instructions can also be found at http://www.elsevier.com/wps/find/journaldescription.cws_home/622898/authorinstructions.

Journal of Solid State Chemistry has no page charges.